applied sciences

MDPI

Article

Performance Study on a Soft X-ray Betatron Radiation Source Realized in the Self-Injection Regime of Laser-Plasma Wakefield Acceleration

Alessandro Curcio [1,*], Alessandro Cianchi [2,3,4], Gemma Costa [5], Francesco Demurtas [2], Michael Ehret [1], Massimo Ferrario [5], Mario Galletti [2,3,4], Danilo Giulietti [6], José Antonio Pérez-Hernández [1] and Giancarlo Gatti [1]

1 Centro de Laseres Pulsados (CLPU), Edificio M5. Parque Científico. C/Adaja, 8, 37185 Villamayor, Spain
2 Department of Physics, Università di Roma Tor Vergata, Via Ricerca Scientifica 1, 00133 Rome, Italy
3 INFN-Tor Vergata, Via Ricerca Scientifica 1, 00133 Rome, Italy
4 Nast Center, Via Ricerca Scientifica 1, 00133 Rome, Italy
5 Laboratori Nazionali di Frascati, Via Enrico Fermi 54, 00044 Frascati, Italy
6 Department of Physics, University of Pisa and INFN, Largo Bruno Pontecorvo 3, 56127 Pisa, Italy
* Correspondence: acurcio@clpu.es

Abstract: We present an analysis of the performance of a broadband secondary radiation source based on a high-gradient laser-plasma wakefield electron accelerator. In more detail, we report studies of compact and ultra-short X-ray generation via betatron oscillations in plasma channels. For the specific working point examined in this paper, determined by the needs of other experiments ongoing at the facility, at ∼0.02 Hz operation rate, we have found $\lesssim 10^6$ photons emitted per shot (with a fluctuation of 50%) in the soft X-rays, corresponding to a critical energy of ∼0.8 keV (with a fluctuation of 40%). The source will be implemented for experiments in time-domain spectroscopy, e.g., biological specimens, and for other applications oriented to medical physics.

Keywords: laser-plasma wakefield acceleration; secondary radiation sources; broadband sources

Citation: Curcio, A.; Cianchi, A.; Costa, G.; Demurtas, F.; Ehret, M.; Ferrario, M.; Galletti, M.; Giulietti, D.; Pérez-Hernández, J.A.; Gatti, G. Performance Study on a Soft X-ray Betatron Radiation Source Realized in the Self-Injection Regime of Laser-Plasma Wakefield Acceleration. *Appl. Sci.* **2022**, *12*, 12471. https://doi.org/10.3390/app122312471

Academic Editor: Detlef Kip

Received: 11 November 2022
Accepted: 1 December 2022
Published: 6 December 2022

1. Introduction

The expression (laser-)plasma wakefield acceleration refers to schemes of charged-particle acceleration exploiting the highly electric fields that are sustainable by plasmas [1–12]. Electric fields in plasmas can exceed the so-called wave-breaking limit for a cold non-relativistic plasma [13,14]:

$$E_{wb} \sim 96 \sqrt{n_e[10^{18}\mathrm{cm}^{-3}]}\ \mathrm{GV/m} \tag{1}$$

where the electron plasma density is denoted by n_e. The term wave-breaking indicates indeed a breakdown phenomenon, the one involving the fronts of the Langmuir waves [15]. Wave-breaking can be responsible for the onset of regions of high-amplitude electric fields, reaching extraordinary values as high as $\lesssim TV/\mathrm{m}$ [16–18]. Langmuir waves, also known as electron plasma waves, are collective oscillations of the electron plasma density. These oscillations can be induced by perturbing the plasma with an external excitation. The external excitation can be realized either through a laser pulse or by means of a bunch of charged particles. In fact, both a laser pulse and a bunch of charged particles can be associated with an electric field $\vec{E}_0$. This driving field can act on the plasma electrons as a collectivity, generating a Langmuir wave in its wake. In the frequency domain, it is possible to establish a relationship between the pumping field $\vec{E}_0$ and the wakefield $\vec{E}$ [19]:

$$\vec{E}(\vec{r},\omega) = \left(\frac{1}{\varepsilon(\omega,\vec{E}_0)} - 1\right) : \vec{E}_0(\vec{r},\omega) \tag{2}$$

where we have introduced the dielectric function of the plasma $\varepsilon(\omega, \vec{E}_0)$. The explicit dependence of the dielectric function upon the driving field is shown with the aim to remind that a non-linear response of the plasma, when excited by high-intensity drivers, must be expected. This also means that the effective driving field may not be directly provided by the pumping field $\vec{E}_0$ (as for the case of an intense laser pulse) but rather a complicated non-linear function of the same field hidden within the dielectric function. Furthermore, the vectorial dependence is also explicitly shown since the plasma response may be anisotropic. Indeed, we have introduced the double dot product ":" due to the fact that, at high intensity, the polarization of the excited wave can be different from that of the pumping field. The latter is particularly true when a high-intensity transversally polarized laser induces a longitudinal (in the direction of light propagation) plasma perturbation through the so-called ponderomotive force [13]. In the self-injection regime, the laser excites plasma wakefields above the wave-breaking threshold in such a way that electrons from the background plasma, concentrated in the region of wave-breaking, can be injected into the wakefield and accelerated spontaneously. Since $1/\varepsilon$ tends to zero for some value of the exciting frequency $\omega \sim \omega_p$, where $\omega_p(\vec{E}_0)$ is the non-linear plasma frequency, the wakefields are efficiently generated when the spectrum of the effective driver extends over the ω_p range. Furthermore, Equation (2) also shows that a resonant plasma excitation ($1/\varepsilon >> 1$) corresponds to a wakefield amplitude that can be orders of magnitude higher than the electric amplitude of the pumping field. In Figure 1, the laser-plasma wakefield (LWFA) accelerator at the CLPU facility (Salamanca, Spain) is shown. The present paper aims to be an overview of the performance of the latter accelerator and of the secondary source of X-rays based on it for a specific working point, i.e., for a particular case of operational conditions. Such conditions were determined by the needs of another experiment ongoing at the facility [20]. Keeping the parameters of the plasma-electron source as they were set for the experiment in [20], the betatron radiation was studied (therefore there was no optimization work on the betatron source but only characterization). The motivation was two-fold: to characterize the background provided by the betatron radiation mechanism to the ongoing experiment, and to individuate the parameters of the betatron source in order to possibly use it in the future as a standalone tool for irradiation and spectroscopy. Experimental data will be reported both concerning the plasma-electron accelerator and the X-ray secondary source. A detailed and correlated analysis of the fluctuations of both the electron and radiation sources will be finally presented, with the goal of explaining the experimental findings by means of scaling laws provided by well-established literature and eventually listing the performance parameters of the betatron source for future use.

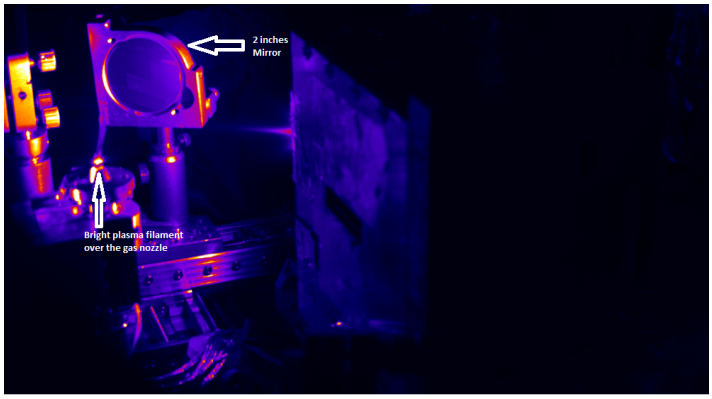

Figure 1. Real image of the VEGA 2 laser-plasma accelerator. The plasma filament is visible above the conical gas nozzle. Given the scale of the picture, the plasma accelerator is as short as a few mm.

2. Fluctuations of the Plasma Source and the Electron Beams

In this section, we present a working point of the VEGA2-based electron source. We stress that a single working point is shown, despite many other operational conditions being available at the facility. This one was found to be the most stable for the type of gas nozzle

and gas species/density adopted. In more detail, a conical gas jet was used, 5 mm long at the exit-plane of the nozzle, along the laser propagation axis (see Figure 2 for the schematics of the experimental setup). The gas used for the experiments was pure helium, therefore the mechanism of electron injection was the pure self-injection. Alternative injection mechanisms can be implemented at the facility, and would give different performances of the electron and relative radiation sources. Future experimental campaigns will be devoted to this aspect. Besides the scenario of exploiting and/or mixing different gases, also different nozzle designs with different lengths, different conical apertures and/or capable of sustaining different density regimes may be considered. We do not go further in this vast topic, since the data presented in this paper refer to a single operational configuration, above described. Furthermore, we present a sequence of 10 shots for each data collected in the campaign, in such a way as to observe and quantify the shot-to-shot fluctuations over a significant amount of acquired data corresponding to 10 min of operation (indeed, the working rep rate was one shot per minute, dictated by the recovery of the vacuum level after shooting the laser on the gas target).

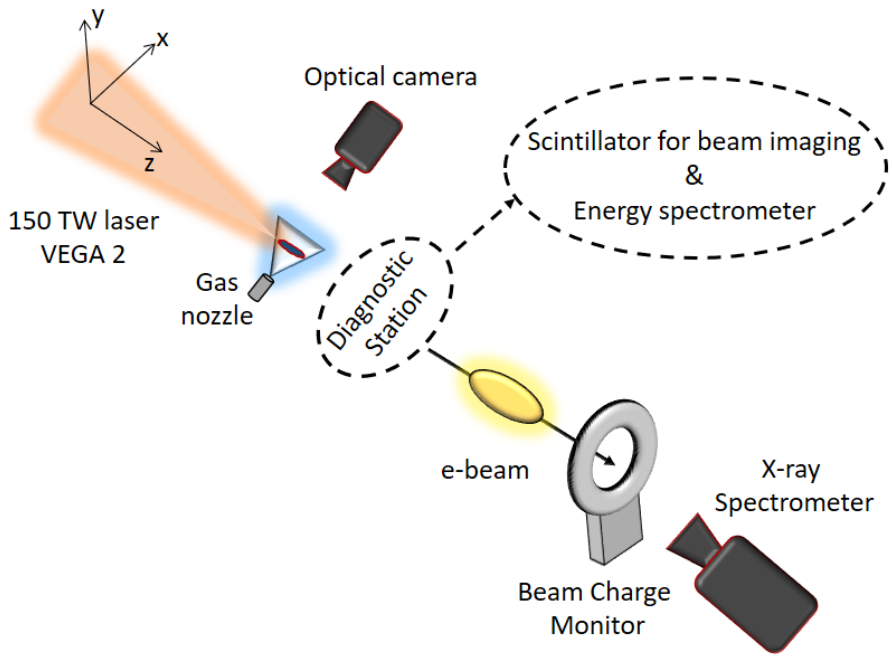

Figure 2. Experimental setup (X-rays detected after deflecting the electrons into the spectrometer).

The plasma filament was studied by means of a visible camera, watching the filament from the top, with an angle of 90°, detecting the light from the plasma, dominated by the mechanism of Thomson scattering. The experimental results are shown in Figure 3. The maximal plasma density is measured starting from the density of neutrals, which is characterized prior to the experiment on a separate interferometric station. The laser intensity is such to ionize the gas completely before the main pulse arrives on target, in such a way that the core laser energy is transferred into the plasma. The laser beam arrives on the nozzle with a height of ∼2 mm with respect to it. The ionization rate over one cycle of the laser field is given by the Landau expression for tunneling ionization [21]:

$$w = 4\omega_a u^{5/2} \frac{E_a}{|E_0|} e^{-\frac{2E_a}{3|E_0|}u^{3/2}} \quad (3)$$

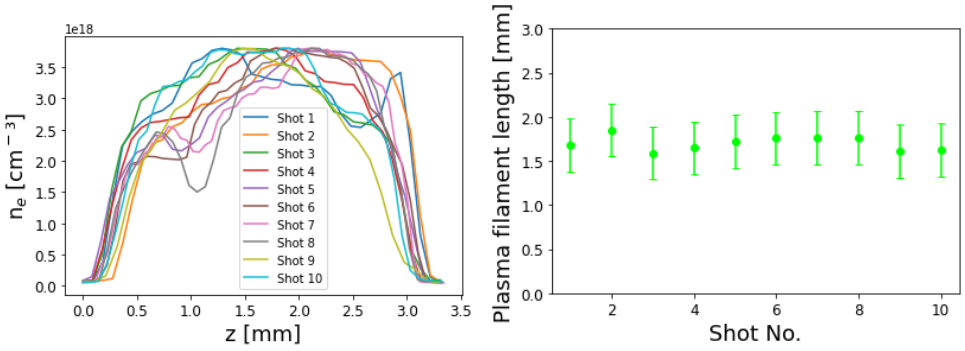

Figure 3. (**Left**): Reconstructed electron plasma density axial profiles from the Thomson scattering optical diagnostics. (**Right**): shot-to-shot fluctuation of the plasma filament length, assumed to be as long as the electron acceleration length; the uncertainty is determined by the resolution of the imaging system.

The quantity u takes into account for a hydrogen-like atom different from hydrogen (for which $u = 1$). Indeed, u is the ratio between the ionization potential of a considered atom/molecule and that of the hydrogen atom/molecule. For *He*, considering the second ionization potential, which is larger than the first, we obtain $u = 4$. The atomic frequency is constantly equal to $\omega_a = 4.134 \times 10^{16}$ rad/s, while the atomic field is $E_a = 5.14$ GV/cm. For an electric field $E_0 \sim 2.7$ GV/cm, corresponding to a laser intensity 10^{16} W/cm^2, within an integration time corresponding to a laser cycle $2\pi/\omega_0$ (for VEGA2 $\omega_0 = 2.35 \times 10^{15}$ rad/s), $\int_0^{2\pi/\omega_0} dtw \simeq 1$, which means that the atom is surely ionized much before interacting with the peak of the laser pulse. The peak intensity of VEGA 2 used for the experiments in this paper was 10^{19} W/cm^2, on average, much larger than 10^{16} W/cm^2, therefore the front tail of the laser pulse was able to fully ionize the helium gas. The first ionization in fact occurs even more easily than the second, because it corresponds to a lower ionization potential (please notice that the approximation of a hydrogen-like atom cannot hold true for the *He* atom, thus the u factor should in that case take into account for the screening effects, but this eventually does not affect the validity of our arguments). The number of photons needed for a single He atom ionization (second ionization) is approximately 35. For a laser beam radius of $\sigma \sim 15$ µm and a propagation length in the plasma of $L \sim 2$ mm we obtain that the total number of atoms involved effectively in the interaction is $n_a \pi \sigma^2 L \simeq 3 \times 10^{12}$, given a neutral density $\sim 2 \times 10^{18}$ cm^{-3}. Thus, the number of photons lost in ionization is $35 \times 3 \times 10^{12} \simeq 10^{14}$. The number of photons carried by a laser pulse with peak intensity of $I_0 \sim 10^{19}$ W/cm^2, corresponding to a laser energy of ∼3 J, 30 fs (FWHM) pulse duration and focal radius $\sigma \sim 15$ µm, is of the order of $N_0 \sim 10^{19}$. This demonstrates that ionization is a loss channel for the laser energy with a branching ratio of $\sim 10^{-5}$, i.e., most of the laser energy is coupled into the plasma. Knowing the maximal density, we can set a scale on the left plot of Figure 3. This is performed also under another consideration: Thomson scattered light is proportional to the local electron plasma density. Even if it remains true that electrons scattering the laser light are located in a region corresponding to a local plasma density higher than the background plasma density (due to the ponderomotive action of the laser pulse-front that accumulates electrons at the head of the pulse), such density must be proportional to the background plasma density (the amount of charge blown by the laser is proportional to the amount of charge available before such interaction). The visible camera can record scattered light at ω_0 and $2\omega_0$, the latter being produced via non-linear Thomson scattering. The amount of power scattered by the unit volume of plasma is therefore found through (for a linearly polarized laser):

$$\frac{dP}{dV} = \frac{n_e I_0 \sigma_T}{1 + \frac{a_0^2}{2}} \left(1 + \frac{a_0^2}{2 + a_0^2} \right) \tag{4}$$

where n_e is the electron plasma density seen by the laser pulse, σ_T is the classical Thomson cross-section, while the terms in $a_0 = eE_0/m\omega_0 c$ are relativistic corrections (m is the electron mass, e is the elementary charge and c is the speed of light in vacuum). In particular, the second term within brackets is associated with the emission of the second harmonic of the laser frequency. The laser beam is guided by relativistic self-focusing in the plasma channel and its energy is depleted in generating strong plasma perturbations, i.e., the plasma wakefields. In the extremely non-linear regime of interaction $a_0 >> 1$, the pump depletion length is $L_{pd} = \omega_0^2 c\tau/\omega_p^2$, with τ the laser pulse length. The plasma frequency is related to the electron plasma density as $\omega_p = \sqrt{n_e e^2/\varepsilon_0 m}$, where the vacuum dielectric constant is ε_0. In our experiment $L_{pd} \simeq 4.1$ mm, which was larger than the average plasma filament length, meaning that the laser was only moderately depleted during the propagation. Moreover, the laser beam envelope oscillations, typical of self-guiding phenomena, could not be properly resolved by the Thomson imaging system. In conclusion, Equation (4) could be used to argue that the amount of light detected locally from the plasma filament was dominated by the electron plasma density more than by the laser beam evolution (unappreciable local intensity changes). In other words, the high-frequency modulations of the scattered light due to laser beam evolution in the filament could not be observed and the low-frequency modulation due to depletion was negligible. The average plasma filament length on the left of Figure 3 was calculated as:

$$L = \frac{\int n_e(z) z dz}{\int n_e(z) dz} \tag{5}$$

where the profiles $n_e(z)$ are given on the right of Figure 3. The average value of 1.7 mm corresponds to the distance along which the laser pulse is relativistically self-guided in the plasma. Given the above assumptions, the axial profile of the accelerating field could be indirectly measured, as shown in Figure 4. In fact, the formula relating the accelerating field to the electron plasma density and laser intensity is found in the literature [14]:

$$E = \frac{mc\sqrt{a_0}\omega_p}{e} \tag{6}$$

On the right of Figure 4 the average gradients of acceleration are reported, in the order of 1.5 GV/cm. The axial profiles of such longitudinal plasma wakefields along the plasma "accelerating cavity" (indirectly reconstructed via Equation (6)) are depicted on the left of Figure 4. When the beam was not magnetically deflected for energy characterization, the bunch charge was measured via a beam charge monitor after the plasma source [20]. The mean charge was around ~370 pC, as shown in Figure 5. The scaling for the bunch charge with the laser peak power P_0 is also found in the literature in the non-linear regime of laser wakefield acceleration [14]:

$$Q[pC] \simeq 400 \frac{\lambda_0}{0.8[\mu m]} \sqrt{\frac{P[TW]}{100}} \tag{7}$$

where the laser wavelength is defined as $\lambda_0 = 2\pi c/\omega_0$. During the experiment, the laser peak power on target was ~100 TW, therefore we had to expect ~400 pC per bunch according to the existing scaling laws. The experimental result was rather in agreement with the expectations. The electron beam profile at the exit of the plasma accelerator is measured by means of a Lanex scintillator screen. The shot-to-shot variation of the mean radial divergence $\sqrt{< \theta_{ex}^2 + \theta_{ey}^2 >}$ (where θ_{ex} is the electron divergence in the horizontal direction, in the same plane of laser propagation and parallel to the polarization direction, and θ_{ey} is the vertical-divergence direction, transverse to the propagation and polarization directions) is reported on the right of Figure 6. A typical electron beam profile is reported on the left of Figure 6. Finally, a typical electron energy spectrum obtained by a magnetic deflector coupled to a Lanex scintillator is depicted on the left of Figure 7. On the right

of the same figure the shot-to-shot variations of energy and energy spreads are reported. The magnetic deflector was composed of a 10 cm long magnet, with field amplitude 1.2 T, coupled to a LANEX scintillator screen 15 cm away from the exit slit of the magnet.

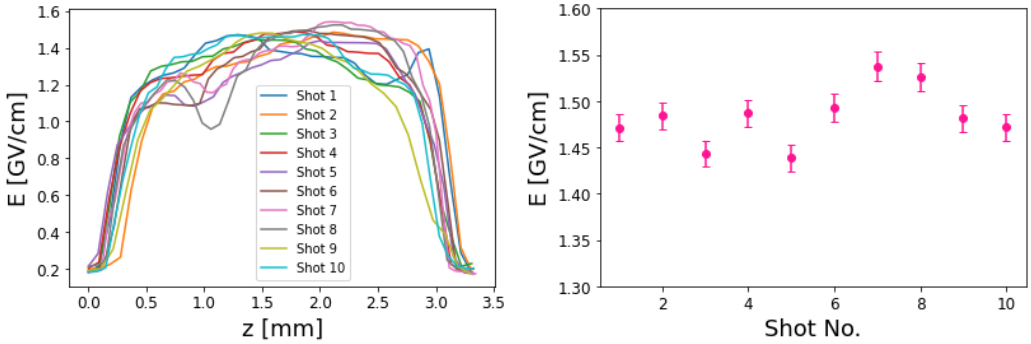

Figure 4. (**Left**): Reconstructed accelerating wakefield axial profiles. (**Right**): shot-to-shot fluctuation of the peak of the longitudinal electric plasma wakefield; the uncertainty is determined by standard deviation of the measurements.

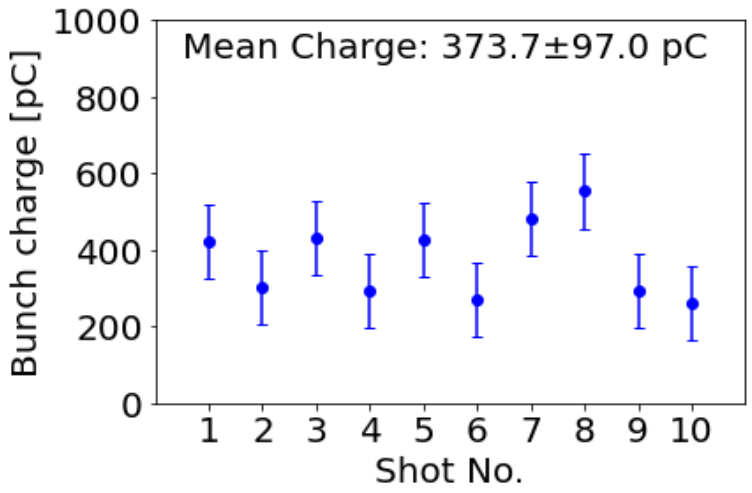

Figure 5. Shot-to-shot fluctuations of the charge of the accelerated electron bunches.

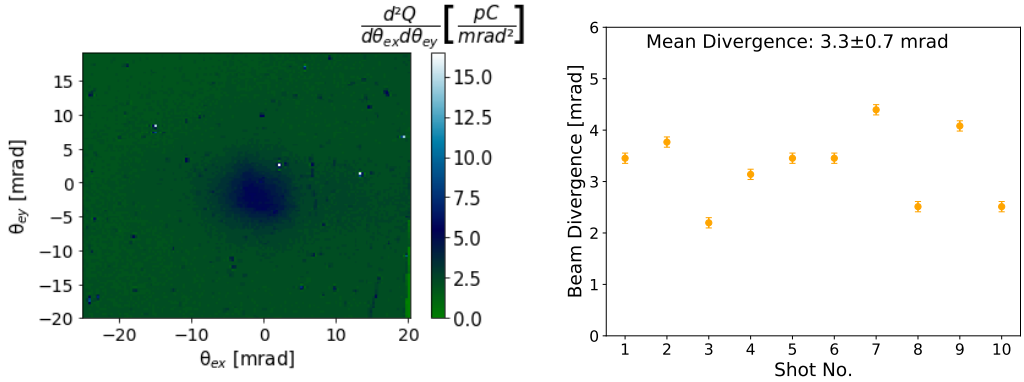

Figure 6. (**Left**): Example of electron beam profile on the diagnostic scintillator, plotted in divergence units (**Right**): shot-to-shot fluctuation of the beam radial divergence; the uncertainty is determined by standard deviation of the measurements.

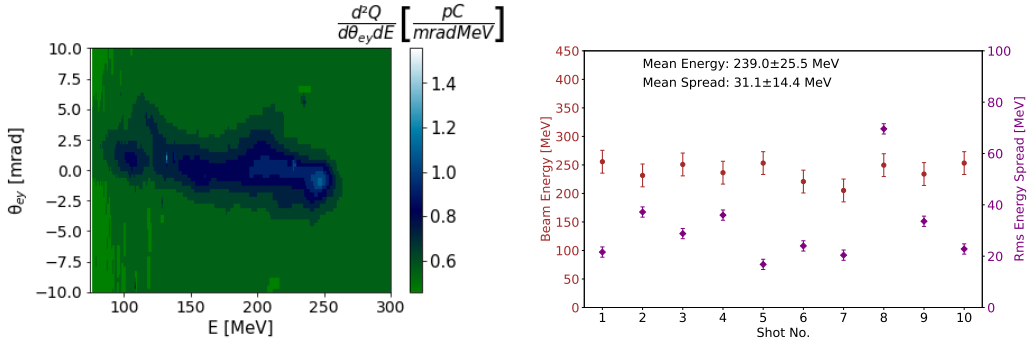

Figure 7. (**Left**): Example of electron beam energy spectrum on the diagnostic scintillator placed after the bending magnet, plotted in vertical-divergence/MeV units (**Right**): shot-to-shot fluctuation of the beam energy and rms energy spread; the uncertainty is determined by standard deviation of the measurements.

3. Betatron Radiation Sources

Plasma wakefield acceleration has also been demonstrated to be a promising platform for producing secondary radiation [22–33]. The compactness of plasma wakefield accelerators is correlated with the shortness of the accelerating buckets so that only very short bunches of particles can be accelerated down to a few femtoseconds [27,28]. This means that the radiation pulses secondarily emitted by these particles will also be short, delivering high peak power. The fact that plasma wakefield accelerators produce for ultra-relativistic electrons also makes possible the emission of intense bursts of light with extremely interesting angular and spectral properties, e.g., the high-energy photon emission within narrow solid angles. Here, we focus on incoherent radiation, which is the case for the radiation emitted in plasma wakefield accelerators by beams undergoing betatron oscillations [22–33]. The radiation field far from the source is found as solution of the Maxwell equations [19]:

$$\vec{H}(\vec{R},\omega) = \frac{\omega}{4\pi c}\frac{e^{i\frac{\omega R}{c}}}{R^2}\vec{R}\times\widetilde{\vec{j}}(\vec{k},\omega) \tag{8}$$

where the observation vector is $\vec{R} = R\{\cos\varphi\sin\theta, \sin\varphi\sin\theta, \cos\theta\}$, with θ the polar angle and φ the azimuth. The Fourier–Laplace transform of the current density $\vec{j}(\vec{r},t) = q\delta(\vec{r}-\vec{r}_e)$ associated with a single electron, whose motion is described by $\vec{r}_e = \vec{r}_e(t)$, evaluated in the spatial-frequency/time domain, is:

$$\vec{j}(\vec{k},t) = q\frac{d\vec{r}_e}{dt}e^{-i\vec{k}\cdot\vec{r}_e} \tag{9}$$

The trajectory of a generic electron injected in the plasma accelerator is given by [33]:

$$\vec{r}_e = \left\{\left(\frac{\gamma_0}{\gamma(t)}\right)^{\frac{1}{4}} x_\beta \sin(\omega_\beta t + \psi_x + \varphi_0), \left(\frac{\gamma_0}{\gamma(t)}\right)^{\frac{1}{4}} y_\beta \sin(\omega_\beta t + \psi_y + \varphi_0), \int_0^t dtc\sqrt{1 - \frac{1}{\gamma^2(t)} - \frac{v_x^2 + v_y^2}{c^2}}\right\} \tag{10}$$

where the velocity of the particle is $\vec{v}_e = \{v_x, z_y, v_z\} = d\vec{r}_e/dt$ and the transverse coordinates (i.e., the first two components of $\vec{r}_e$, since we have chosen z as beam axis) represent the so-called betatron oscillations occurring at frequency $\omega_\beta = \omega_p/\sqrt{2\gamma(t)}$. The Lorentz factor of the particle gaining energy from the plasma wakefield is $\gamma(t)$, while γ_0 is the initial value for the same particle at the injection plane. The phase shift, related to initial injection condition for the electron, is for the two planes:

$$\psi_{x,y} = \arctan\left[\left(\frac{\gamma_0}{\gamma(t)}\right)^{\frac{1}{4}}\frac{\{x_\beta, y_\beta\}\omega_\beta}{c\theta_{x,y}}\right] \tag{11}$$

where $\theta_{x,y} = v_{x,y}/v_z$ is the injection angle of the electron into the plasma wakefield. With writing $\{x_\beta, y_\beta\}$ we mean "either x_β or y_β, according whether the x or the y direction is considered, respectively". The phase ϕ_0 is instead the phase retardation with respect to a reference particle, which accounts for the fact that not all particles are injected at the same time. All the above equations make a self-consistent set to calculate the number of photons dN emitted in the frequency bandwidth $d\omega$, through the Lienard–Wiecher formula [34] starting from the magnetic field at Equation (8):

$$\frac{dN}{d\omega} = \frac{q^2\omega}{16\pi^3\varepsilon_0\hbar c^3}\int d\Omega dx_\beta dy_\beta d\theta_x d\theta_y d\phi_0 d\gamma_0 \rho_{beam}\left|\frac{\vec{R}}{R}\times\int_{t+\frac{\phi_0}{\omega_\beta}}^{L/c} dt\vec{v}(t)e^{i\omega t-\vec{k}\cdot\vec{r}_e}\right|^2 \quad (12)$$

where $\rho_{beam} = \rho_{beam}(x_\beta, y_\beta, d\theta_x, d\theta_y, \phi_0, \gamma_0)$ is the trace space density of the particle beam at the injection plane. The lower limit of the time integral must depend on ϕ_0, since in injection schemes as the self-injection the particles can be continuously injected all through the laser propagation in the plasma, so that they can have very different acceleration lengths (this is source of energy spread at the end of the acceleration process). Despite Equation (12) not being possible to be solved analytically, in general, asymptotic limits can be guessed for particles such that $\gamma v_{x,y}/c >> 1$. In that case, $v_{x,y}\exp(i\omega t - \vec{k}\cdot\vec{r}_e) \propto K_{2/3}(\omega/\omega_c)$ for radiation emitted on axis. The modified Bessel function $K_n(x)$ of the second kind presents a parameter called critical energy ω_c, determining the shape of the betatron spectrum. For synchrotron radiation, the same parameter divides the spectrum in two regions, each carrying half of the total energy irradiated. Choosing a description of the betatron spectrum as a synchrotron-like spectrum, we expect for high-frequencies ($\omega >> \omega_c$) that $dN/d\omega \propto e^{-\omega/\omega_c}$. Figure 8 shows experimental data of measured betatron spectra at VEGA 2. The critical energies reported in the legend $E_c = \hbar\omega_c$ have been fitted with the exponential function introduced above. The curves have been represented in order of consecutive shots, where a higher critical energy does not necessarily correspond to a higher number of emitted photons due to the fluctuations of other experimental parameters. The most critical parameter determining instability for critical energy is the electron energy, since critical energy scales non-linearly with it. In the following, we provide the scaling of critical energy upon all the experimental parameters. Experimentally, a shot-to-shot fluctuation of E_c up to 40% has been observed. An expression for this parameter can be found [28,33]:

$$E_c = \frac{3}{2}\hbar\gamma^3(t)\left(\frac{\gamma_0}{\gamma(t)}\right)^{\frac{1}{4}}\frac{\{x_\beta, y_\beta\}\omega_\beta^2}{c} \propto \gamma(t)^{\frac{7}{4}}n_e \quad (13)$$

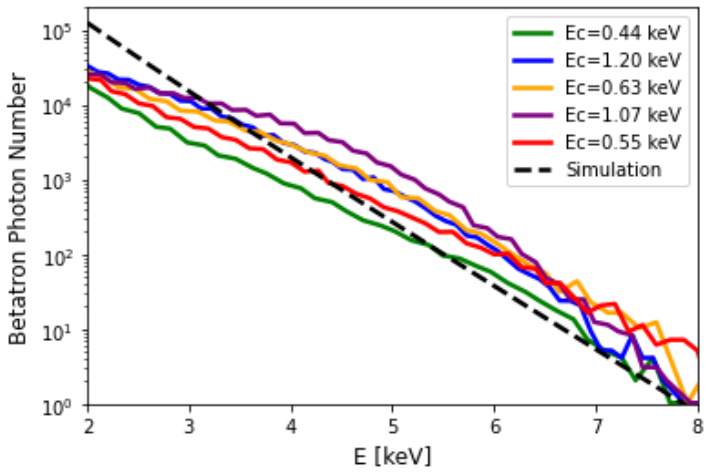

Figure 8. Measurements of betatron radiation spectra. For "Betatron Photon Number", $\sim(dN/d\omega)\times\Delta\omega$ with $\Delta\omega = 0.13\,keV$, which the resolution of the diagnostic apparatus.

A fluctuation of the mean energy ∼10%, such as that shown by the data of Figure 7, together with an energy spread of 13%, is translated already in a critical energy fluctuation of ∼40%. Adding the measured density fluctuation of 5% would not change the result much; therefore, we believe that the main sources of critical energy instability were the energy gain and the energy spread of the electron beam. Moreover, in the above reasoning, we neglected fluctuations of the betatron oscillation amplitudes, which apparently are also less important than the energy/spread fluctuations, since the latter can already explain the observed shot-to-shot variation of the critical energy of the betatron spectrum. The mean critical energy for the shots in Figure 8 was 0.78 keV. We consider a quadratic energy gain, as in [33], and averaging Equation (13) on the acceleration length we can infer an effective value (one for both directions) for the betatron oscillation amplitude equal to ∼0.2 µm, where in Equation (13) we have replaced E_c with the measured mean value of 0.78 keV as well as replacing $\gamma(L/c) \simeq 468$ given the results in Figure 7. Figure 8 also shows a simulation performed using analytical formulas of synchrotron-like betatron radiation, including electron acceleration [33]. The parameters used for the simulation have been: rms betatron oscillation amplitude equal to ∼0.2 µm (gaussian beam), electron final Lorentz factor at $z = L = 1.7$ mm equal to 468, and finally the laser and plasma parameters used in the experiment. The effect of the electron energy spectrum and of the radial distribution of the beam has been obtained by summing incoherently the betatron radiation emission from a statistical sample of 10,000 electrons, representing the total charge of 373 pC. The simulation is reasonably in agreement with the results, even if the synchrotron-like approximation seems to overestimate the low-energy photons. The mean number of measured photons per shot in the range >2 keV was $\sim 4 \times 10^5$, with a fluctuation of the 50 %. The detector response (a CCD X-ray camera operated in single photon counting) for lower photon energies was not reliable so it was neglected, due to thermal noise. The used camera was a Great Eyes 1024 256, with an image area of 26.6 mm × 6.7 mm, a pixel size of 26 µm × 26 µm, operated at a pixel readout frequency of 500 kHz and a temperature of the sensor equal to −20°. The algorithm used to retrieve the photon spectrum has been based on the determination of isolated illuminated pixels on the sensor matrix and in the construction of the histogram of their values. This algorithm can lead to a slight underestimation of photons, in general, but this was not the case in our experiment, as no significant contiguous events were detected on the sensor. The process has been implemented after background subtraction and considering only photons above the thermal noise threshold. Moreover, a deconvolution with the transmission function of 2 µm thick Al window in front of the sensor (to reflect spurious laser light preventing the sensor damage) has been performed. If simulated within a synchrotron-like approximation, as in shown in Figure 8, the number of measured photons would correspond to 1% of the total photon number, which is $\lesssim 10^8$. The missing photons, constituting the majority of emitted radiation, have not been detected as they fell below 2 keV. The scaling for the total photon number can be expressed as [33]:

$$N_\beta = \left(\frac{\gamma_0}{\gamma(t)}\right)^{\frac{1}{4}} \frac{2\pi\alpha Q\{x_\beta, y_\beta\}\omega_p^2 L}{18ec^2} \propto Q n_e L \gamma^{-\frac{1}{4}} \tag{14}$$

Considering the fluctuations of the quantities upon which the betatron photon number scales, we obtain an overall fluctuation ∼45 %, which explains rather well the observed results (still neglecting the fluctuations on the betatron oscillation amplitudes). Once evaluated for the parameters of our experiment, Equation (14) yields a photon number $\lesssim 10^8$ for a betatron amplitude ∼0.2 µm, which is in agreement with our previous estimation based on a simulation of a synchrotron-like spectrum (see Figure 8).

4. Discussion

We would like to stress that our working point at $E_c \lesssim 1$ keV is unique in the literature, since most of the previous works and published papers show critical energies on the

several to many keVs level. With a more appropriate UV detector, we would have been able to detect ultra-short bursts of ultraviolet radiation, demonstrating a promising radiation source in that range of frequencies. However, our experimental conditions are quite well explained by scaling laws found in the literature, as discussed in the previous section. Concerning the literature, we also would like to recall that with a similar laser system, with a longer off-axis parabola, and similar conditions for plasma density and injection scheme, other authors have demonstrated the same electron energies but higher critical energy (in the few keVs) and number of photons ($\sim 10^8$) [26]. In another work, with a similar experimental setup, larger electron energies up to 500 MeV have been demonstrated and larger critical energies of the betatron spectrum up to $\lesssim$10 keV [35], but smaller bunch charges. The reason for these differences may be attributed to different conditions for laser guiding and/or different injection schemes realized, e.g., with a mixture of gases, affecting the electron beam emittance, the bunch charge and the energy spread. A similar photon number but higher critical energy has been obtained in [36], obtained with a slightly longer off-axis parabola and higher electron plasma density. In conditions of direct laser–electron interaction, the critical energy may be even shifted towards γ-rays [30,37,38]. With comparable laser intensity but different systems with longer pulses, different regimes have been studied, as the self-modulated regime [39], demonstrating large photon number and critical energies on the tens of keVs. Further enhancing techniques for photon number and critical energy are based on the addition of wiggling sources and/or density tailoring [31,32,40–45] or with different gas targets [46,47].

5. Conclusions

We have reported a detailed study on a high-gradient laser-plasma accelerator and its related synchrotron-like source. Diagnostic methods based on Thomson scattering allowed the reconstruction of the accelerating field axial profile and amplitude. Electron and photon numbers, as well as their spectral-angular characteristics, have been measured and explained through the established literature, with particular focus on the fluctuation theory of such observables. For the operational conditions considered here, driven by an ongoing experiment at the facility, with a $\sim$0.02 Hz operation rate, we have found $\lesssim 10^6$ photons emitted per shot (with a fluctuation of 50%) in the soft X-ray range, corresponding to a critical energy of $\sim$0.8 keV (with a fluctuation of 40%). Future developments will be needed for improving and/or expanding the above performances, especially with the aim of extending the range of applications of the betatron radiation source.

Author Contributions: Conceptualization, A.C. (Alessandro Curcio); Methodology, M.G.; Investigation, A.C. (Alessandro Curcio), G.C., F.D., M.E. and J.A.P.-H.; Data curation, A.C. (Alessandro Curcio); Writing—original draft, A.C. (Alessandro Curcio); Writing—review & editing, A.C. (Alessandro Cianchi) and D.G.; Visualization, G.C., F.D., M.E., M.F., M.G., D.G., J.A.P.-H. and G.G.; Supervision, A.C. (Alessandro Cianchi), M.F. and G.G. All authors have read and agreed to the published version of the manuscript.

Funding: The research leading to these results has received funding from LASERLAB-EUROPE V (Grant Agreement No. 871124, European Union Horizon 2020 research and innovation program). This work has also been partially supported by the EU Commission in the Seventh Framework Program, Grant Agreement 312453-EuCARD-2 and the European Union Horizon 2020 research and innovation program, Grant Agreement No. 653782 (EuPRAXIA)

Data Availability Statement: The data that support the findings of this study are available from the corresponding author on reasonable request.

Conflicts of Interest: The authors declare no conflict of interest.

References

1. Tajima, T.; Dawson, J.M. Laser electron accelerator. *Phys. Rev. Lett.* **1979**, *434*, 267. [CrossRef]
2. Curcio, A.; Giulietti, D. *Laser-Plasma Acceleration and Secondary em Radiation*; Aracne: Rome, Italy, 2019.

3. Hogan, M.J.; Raubenheimer, T.O.; Seryi, A.; Muggli, P.; Katsouleas, T.; Huang, C.; Lu, Y.; An W.; Marsh, K.A.; Mori, W.B.; et al. Plasma wakefield acceleration experiments at FACET. *New J. Phys.* **2010**, *12*, 055030. [CrossRef]
4. Barov, N.; Rosenzweig, J.B.; Conde, M.E.; Gai, W.; Power, J.G. Observation of plasma wakefield acceleration in the underdense regime. *Phys. Rev. Spec.-Top. Beams* **2000**, *3*, 011301. [CrossRef]
5. Loisch, G.; Asova, G.; Boonpornprasert, P.; Brinkmann, R.; Chen, Y.; Engel, J.; Good, J.; Gross, M.; Grüner, F.; Huck, H.; et al. Observation of high transformer ratio plasma wakefield acceleration. *Phys. Rev. Lett.* **2018**, *121*, 064801. [CrossRef]
6. Amiranoff, F.; Baton, S.; Bernard, D.; Cros, B.; Descamps, D.; Dorchies, F.; Jacquet, F.; Malka, V.; Marquès, J.R.; Matthieussent, G.; et al. Observation of laser wakefield acceleration of electrons. *Phys. Rev. Lett.* **1998**, *81*, 995. [CrossRef]
7. Lifschitz, A.F.; Faure, J.; Malka, V.; Mora, P. GeV wakefield acceleration of low energy electron bunches using petawatt lasers. *Phys. Plasmas* **2005**, *12*, 093104. [CrossRef]
8. Chen, P.; Dawson, J.M.; Huff, R.W.; Katsouleas, T. Acceleration of electrons by the interaction of a bunched electron beam with a plasma. *Phys. Rev. Lett.* **1985**, *54*, 693. [CrossRef]
9. Nakajima, K.; Kawakubo, T.; Nakanishi, H.; Ogata, A.; Kato, Y.; Kitagawa, Y.; Kodama, R.; Mima, K.; Shiraga, H.; Suzuki, K.; et al. A proof-of-principle experiment of laser wakefield acceleration. *Phys. Scr.* **1994**, *1994*, 61. [CrossRef]
10. Giulietti, D.; Galimberti, M.; Giulietti, A.; Gizzi, L.A.; Numico, R.; Tomassini, P.; Borghesi, M.; Malka, V.; Fritzler, S.; Pittman, M.; et al. Production of ultracollimated bunches of multi-MeV electrons by 35 fs laser pulses propagating in exploding-foil plasmas. *Phys. Plasmas* **2002**, *9*, 3655–3658. [CrossRef]
11. Zhang, X.; Tajima, T.; Farinella, D.; Shin, Y.; Mourou, G.; Wheeler, J.; Taborek, P.; Chen, P.; Dollar, F.; Shen, B. Particle-in-cell simulation of X-ray wakefield acceleration and betatron radiation in nanotubes. *Phys. Rev. Accel. Beams* **2016**, *19*, 101004. [CrossRef]
12. Blumenfeld, I.; Clayton, C.E.; Decker, F.J.; Hogan, M.J.; Huang, C.; Ischebeck, R.; Iverson, R.; Joshi, C.; Katsouleas, T.; Kirby, N.; et al. Energy doubling of 42 GeV electrons in a metre-scale plasma wakefield accelerator. *Nature* **2007**, *445*, 741–744. [CrossRef]
13. Esarey, E.; Schroeder, C.B.; Leemans, W.P. Physics of laser-driven plasma-based electron accelerators. *Rev. Mod. Phys.* **2009**, *81*, 1229. [CrossRef]
14. Lu, W.; Huang, C.; Zhou, M.; Tzoufras, M.; Tsung, F.S.; Mori, W.B.; Katsouleas, T. A nonlinear theory for multidimensional relativistic plasma wave wakefields. *Phys. Plasmas* **2006**, *13*, 056709. [CrossRef]
15. Chen, F.F. *Introduction to Plasma Physics and Controlled Fusion*; Plenum Press: New York, NY, USA, 1984; Volume 1.
16. Oubrerie, K.; Leblanc, A.; Kononenko, O.; Lahaye, R.; Andriyash, I.A.; Gautier, J.; Goddet, J.-P.; Martelli, L.; Tafzi, A.; Phuoc, K.T.; et al. Controlled acceleration of GeV electron beams in an all-optical plasma waveguide. *Light. Sci. Appl.* **2022**, *11*, 1–7. [CrossRef] [PubMed]
17. Zhu, X.L.; Chen, M.; Weng, S.M.; Yu, T.P.; Wang, W.M.; He, F.; Sheng, Z.-M.; McKenna, P.; Jaroszynski, D.A.; Zhang, J. Extremely brilliant GeV γ-rays from a two-stage laser-plasma accelerator. *Sci. Adv.* **2020**, *6*, eaaz7240. [CrossRef] [PubMed]
18. Gonsalves, A.J.; Nakamura, K.; Daniels, J.; Benedetti, C.; Pieronek, C.; de Raadt, T.C.H; Steinke, S.; Bin, J.H.; Bulanov, S.S.; van Tilborg, J.; et al. Petawatt laser guiding and electron beam acceleration to 8 GeV in a laser-heated capillary discharge waveguide. *Phys. Rev. Lett.* **2019**, *122*, 084801. [CrossRef] [PubMed]
19. Karlovets, D.V.; Potylitsyn, A.P. Universal description for different types of polarization radiation. *arXiv* **2009**, arXiv:0908.2336.
20. Curcio, A.; Ehret, M.; Perez-Hernandez, J.A.; Gatti, G. Observation of tunable parametric X-ray radiation emitted by laser-plasma electron beams interacting with crystalline structures. *Phys. Rev. Accel. Beams* **2022**, *25*, 063403. [CrossRef]
21. Landau, L.D.; Lifshitz, E.M. *Quantum Mechanics: Non-Relativistic Theory*; Elsevier: Amsterdam, The Netherlands, 2013; Volume 3.
22. Esarey, E.; Shadwick, B.A.; Catravas, P.; Leemans, W.P. Synchrotron radiation from electron beams in plasma-focusing channels. *Phys. Rev. E* **2002**, *65*, 056505. [CrossRef]
23. Kostyukov, I.; Kiselev, S.; Pukhov, A. X-ray generation in an ion channel. *Phys. Plasmas* **2003**, *10*, 4818–4828. [CrossRef]
24. Curcio, A.; Anania, M.; Bisesto, F.; Chiadroni, E.; Cianchi, A.; Ferrario, M.; Filippi, F.; Giulietti, D.; Marocchino, A.; Mira, F.; et al. First measurements of betatron radiation at FLAME laser facility. *Nucl. Instrum. Methods Phys. Res. Sect. B Beam Interact. Mater. Atoms* **2017**, *402*, 388–392. [CrossRef]
25. Curcio, A.; Anania, M.; Bisesto, F.; Chiadroni, E.; Cianchi, A.; Ferrario, M.; Filippi, F.; Giulietti, D.; Marocchino, A.; Petrarca, M.; et al. Trace-space reconstruction of low-emittance electron beams through betatron radiation in laser-plasma accelerators. *Phys. Rev. Accel. Beams* **2017**, *20*, 012801. [CrossRef]
26. Fourmaux, S.; Corde, S.; Phuoc, K.T.; Leguay, P.M.; Payeur, S.; Lassonde, P.; Gnedyuk, S.; Lebrun, G.; Fourment, C.; Malka, V.; et al. Demonstration of the synchrotron-type spectrum of laser-produced Betatron radiation. *New J. Phys.* **2011**, *13*, 033017. [CrossRef]
27. Ta Phuoc, K.; Fitour, R.; Tafzi, A.; Garl, T.; Artemiev, N.; Shah, R.; Albert, F.; Boschetto, D.; Rousse, A.; Kim, D.-E.; et al. Demonstration of the ultrafast nature of laser produced betatron radiation. *Phys. Plasmas* **2007**, *14*, 080701. [CrossRef]
28. Curcio, A.; Gatti, G. Time-domain study of the synchrotron radiation emitted from electron beams in plasma focusing channels. *Phys. Rev. E* **2022**, *105*, 025201. [CrossRef] [PubMed]
29. Schnell, M.; Sävert, A.; Landgraf, B.; Reuter, M.; Nicolai, M.; Jäckel, O.; Peth, C.; Thiele, T.; Jansen, O.; Pukhov, A.; et al. Deducing the electron-beam diameter in a laser-plasma accelerator using X-ray betatron radiation. *Phys. Rev. Lett.* **2012**, *108*, 075001. [CrossRef] [PubMed]
30. Curcio, A.; Giulietti, D.; Dattoli, G.; Ferrario, M. Resonant interaction between laser and electrons undergoing betatron oscillations in the bubble regime. *J. Plasma Phys.* **2015**, *81*, 495810513. [CrossRef]

31. Yu, C.; Liu, J.; Wang, W.; Li, W.; Qi, R.; Zhang, Z.; Qin, Z.; Liu, J.; Fang, M.; Feng, K.; et al. Enhanced betatron radiation by steering a laser-driven plasma wakefield with a tilted shock front. *Appl. Phys. Lett.* **2018**, *112*, 133503. [CrossRef]
32. Ta Phuoc, K.; Esarey, E.; Leurent, V.; Cormier-Michel, E.; Geddes, C.G.R.; Schroeder, C.B.; Rousse, A.; Leemans, W.P. Betatron radiation from density tailored plasmas. *Phys. Plasmas* **2008**, *15*, 063102. [CrossRef]
33. Corde, S.; Phuoc, K.T.; Lambert, G.; Fitour, R.; Malka, V.; Rousse, A.; Beck, A.; Lefebvre, E. Femtosecond X rays from laser-plasma accelerators. *Rev. Mod. Phys.* **2013**, *85*, 1. [CrossRef]
34. Jackson, J.D. Classical electrodynamics. *Am. J. Phys.* **1999**, *67*, 841. [CrossRef]
35. Kroupp, E.; Tata, S.; Wan, Y.; Levy, D.; Smartsev, S.; Levine, E.Y.; Seemann, O.; Adelberg, M.; Piliposian, R.; Queller, T.; et al. Commissioning and first results from the new 2× 100 TW laser at the WIS. *Matter Radiat. Extrem.* **2022**, *7*, 044401. [CrossRef]
36. Rousse, A.; Phuoc, K.T.; Shah, R.; Pukhov, A.; Lefebvre, E.; Malka, V.; Kiselev, S.; Burgy, F.; Rousseau, J.-P.; Umstadter, D.; et al. Production of a keV X-ray beam from synchrotron radiation in relativistic laser-plasma interaction. *Phys. Rev. Lett.* **2004**, *93*, 135005. [CrossRef]
37. Huang, T.W.; Robinson, A.P.L.; Zhou, C.T.; Qiao, B.; Liu, B.; Ruan, S.C.; He, X.T.; Norreys, P.A. Characteristics of betatron radiation from direct-laser-accelerated electrons. *Phys. Rev. E* **2016**, *93*, 063203. [CrossRef] [PubMed]
38. Cipiccia, S.; Islam, M.R.; Ersfeld, B.; Shanks, R.P.; Brunetti, E.; Vieux, G.; Yang, X.; Issac, R.C.; Wiggins, S.M.; Welsh, G.H.; et al. Gamma-rays from harmonically resonant betatron oscillations in a plasma wake. *Nat. Phys.* **2011**, *7*, 867–871. [CrossRef]
39. Albert, F.; Lemos, N.; Shaw, J.L.; King, P.M.; Pollock, B.B.; Goyon, C.; Schumaker, W.; Saunders, A.M.; Marsh, K.A.; Pak, A.; et al. Betatron X-ray radiation in the self-modulated laser wakefield acceleration regime: Prospects for a novel probe at large scale laser facilities. *Nucl. Fusion* **2018**, *59*, 032003. [CrossRef]
40. Lee, S.; Lee, T.H.; Gupta, D.N.; Uhm, H.S.; Suk, H. Enhanced betatron oscillations in laser wakefield acceleration by off-axis laser alignment to a capillary plasma waveguide. *Plasma Phys. Control. Fusion* **2015**, *57*, 075002. [CrossRef]
41. Du, B.; Wang, X.F. Influence of an external axial magnetic field on betatron radiation from the interaction of a circularly polarized laser with plasma. *Phys. Plasmas* **2017**, *24*, 093106. [CrossRef]
42. Nam, I.; Hur, M.S.; Uhm, H.S.; Hafz, N.A.; Suk, H. Controlling the betatron oscillations of a wakefield-accelerated electron beam by temporally asymmetric laser pulses. *Phys. Plasmas* **2011**, *18*, 043107. [CrossRef]
43. Guo, B.; Cheng, Z.; Liu, S.; Ning, X.N.; Zhang, J.; Pai, C.H.; Hua, J.F.; Chu, H.H.; Wang, J.; Lu, W. Enhancement of laser-driven betatron X-rays by a density-depressed plasma structure. *Plasma Phys. Control. Fusion* **2019**, *61*, 035003. [CrossRef]
44. Ferri, J.; Davoine, X. Enhancement of betatron X rays through asymmetric laser wakefield generated in transverse density gradients. *Phys. Rev. Accel. Beams* **2018**, *21*, 091302. [CrossRef]
45. Lamač, M.; Chaulagain, U.; Jurkovič, M.; Nejdl, J.; Bulanov, S.V. Two-color nonlinear resonances in betatron oscillations of laser accelerated relativistic electrons. *Phys. Rev. Res.* **2021**, *3*, 033088. [CrossRef]
46. Lécz, Z.; Andreev, A.; Hafz, N. Substantial enhancement of betatron radiation in cluster targets. *Phys. Rev. E* **2020**, *102*, 053205. [CrossRef] [PubMed]
47. Chen, L.M.; Yan, W.C.; Li, D.Z.; Hu, Z.D.; Zhang, L.; Wang, W.M.; Hafz, N.; Mao, J.Y.; Huang, K.; Ma, Y.; et al. Bright betatron X-ray radiation from a laser-driven-clustering gas target. *Sci. Rep.* **2013**, *3*, 1–5. [CrossRef] [PubMed]